Journal Pre-proof

New insights into the analysis of red blood cells from leukemia and anemia patients: Nonlinear quantifiers, fractal mathematics, and Wavelet Transform

Santiago A. Bortolato, Manuel A. Mancilla Canales, Bibiana D. Riquelme, Mariana Raviola, Alcides J. Leguto, Juan P. Rebechi, Patricia Ponce de León, Ana M. Korol

Please cite this article as: S.A. Bortolato, M.A. Mancilla Canales, B.D. Riquelme et al., New insights into the analysis of red blood cells from leukemia and anemia patients: Nonlinear quantifiers, fractal mathematics, and Wavelet Transform, *Physica A* (2020), doi: https://doi.org/10.1016/j.physa.2020.125645.

This is a PDF file of an article that has undergone enhancements after acceptance, such as the addition of a cover page and metadata, and formatting for readability, but it is not yet the definitive version of record. This version will undergo additional copyediting, typesetting and review before it is published in its final form, but we are providing this version to give early visibility of the article. Please note that, during the production process, errors may be discovered which could affect the content, and all legal disclaimers that apply to the journal pertain.

NEW INSIGHTS INTO THE ANALYSIS OF RED BLOOD CELLS FROM LEUKEMIA AND ANEMIA PATIENTS: NONLINEAR QUANTIFIERS, FRACTAL MATHEMATICS, AND WAVELET TRANSFORM

Santiago A. Bortolato[a,c], Manuel A. Mancilla Canales[a,b], Bibiana D. Riquelme[b], Mariana Raviola[a], Alcides J. Leguto[a], Juan P. Rebechi[a], Patricia Ponce de León [a] and Ana M. Korol[a,b]

Revised version

[a] *Facultad de Ciencias Bioquímicas y Farmacéuticas, Universidad Nacional de Rosario, Suipacha 570 Rosario, Argentina.*

[b] *Instituto de Física Rosario (IFIR), CONICET, Ocampo y Esmeralda, Rosario, Argentina.*

[c] *Instituto de Química Rosario (IQUIR), CONICET, Suipacha 570, Rosario, Argentina.*

Abstract

The alterations of red blood cells (RBCs) membrane in many hematological diseases prevent blood to accomplish its functions, but how these alterations occur is not completely understood. Hence, the development of a simple and accurate methodology for the characterization of different populations of RBCs is necessary for hematology and clinical diagnosis. In this work, we focus on different pathologies that affect the hemorheological properties of human beings blood. The results were obtained by studying healthy individuals, anemia and leukemia patient samples. Data analysis involved the use of non-linear methods, based on two different analytical strategies. On one hand, we used nonlinear mathematical quantifiers (False Nearest Neighbors, Embedding Dimension, May-Sugihara Correlation, and Hurst Exponent) on ektacytometrically recorded time series measuring the elongation of re-suspended RBCs subjected to well-defined shear stress. On the other hand, we developed an analytical methodology to aid in the diagnosis of those pathologies, based on the box-counting dimension from digital images of cells suspensions that were denoised standardly by application of Wavelet Transform. The results allowed preliminary discrimination of different populations studied and a correlation with its membrane damage.

Keywords: Hurst Exponent, May and Sugihara, Box-counting dimension, anemia, leukemia, red blood cells.

1 INTRODUCTION

Blood is a type of connective tissue with several biological functions, most of them carried out by the blood cells. White blood cells, or leucocytes, are related to functions of the immune system, while red blood cells (RBCs), or erythrocytes, have as their primary function the transport of oxygen and carbon dioxide. For this, RBCs have to travel through capillaries of diameters smaller than themselves, which leads to a noticeable change in their structure. Consequently, RBCs have unique mechanical properties, which assign them a primary role in determining the rheological behavior of blood [1].

It has been reported that several diseases alter the rheological properties of erythrocytes. Apparently, those changes are responsible for other related pathologies [2,3]. The present report focuses on the effects that leukemia and anemia produce on RBCs membranes. Our research hypothesis holds that while anemia causes biochemical changes that lead directly to a distortion of the membrane of RBCs, leukemia has a different mechanism of action, which triggers distinct biological processes that also lead to alterations of the erythrocyte membranes.

Leukemia is a cancer of the bone marrow and blood, which is classified into four main types: acute myeloid leukemia, chronic myeloid leukemia, acute lymphocytic leukemia (ALL), and chronic lymphocytic leukemia (CLL). Unlike acute leukemia, that evolves quickly and affects cells that have not fully developed, chronic leukemia tends to progress more slowly, inducing an excessive production of relatively mature white blood cells. In general, these more mature cells can perform some of their normal functions, but they can induce symptoms several months after the early stages of the disease. For acute myeloid leukemia, the cancerous alteration begins in a cell in the bone marrow that normally forms RBCs, some types of white blood cells and platelets. Miller and co-workers have reported that this type of leukemia can arise from degenerated RBCs, which also may manifest morphological alterations [4]. In the case of CLL or ALL, a direct correlation between this disease and the morphological alteration of RBCs is not found. Nonetheless, several chronic diseases can injury the membrane of RBCs by hyperthermia or when passing through injured tissues, as already shown [5].

Then, it could be expected a difference between lymphocytic leukemias according to the cell growth rate: for CLL, it should be noted a positive correlation among the disease and viscoelastic alterations of RBC, while for ALL that correlation should be insignificant.

Anemia is a disease promoted by a decrease in the amount of hemoglobin in the blood. Particularly, iron-deficiency anemia (IDA) is a type caused by lack of iron, an indispensable cofactor of hemoglobin. Symptoms are often dubious at early stages of the disease, and include shortness of breath or poor ability to exercise. As anemia evolves, most notorious symptoms appear, such as confusion or feeling like one is going to pass out. In the last decade, a study shows that the decrease of RBCs during anemia can be attributed to an increase in membrane stiffness [6]. This would decrease their deformability, and reduces the ability of the RBCs to pass through the spleen without being removed [6].

According to both the experimental data and the approach to use, a range of innovative concepts is used to describe the manifestation of the complex behavior related to RBCs membranes. For a first approach, we applied techniques of Time Delay Coordinates suggested by Takens [7], False Nearest Neighbors proposed by Abarbanel and co-workers [8], correlation coefficient proposed by May and Sugihara [9], and Hurst Exponent [10]. While the second approach is based on fractal geometry [11], and wavelet transform [12] to analyze fractal patterns measured at different portions of digital images of RBCs. As discussed below, these techniques enable the discrimination of different groups according to their nature.

Our working group has some experience in the use of the nonlinear quantifiers mentioned so far. In fact, we demonstrated how larval parasites interact with RBCs to generate an altered erythrocyte aggregation through fractal geometry measures or analyzing the Brownian motion from these cells under shear stress in a steady state [13,14]. Indeed, these developments are in line with others that use fractal geometry to make a quantitative description of the erythrocyte aggregation phenomena [15,16].

Concerning the first approach, that for simplicity we will call **MSH**, it requires obtaining a time series that account for the alteration of the erythrocyte membranes. The assumption is that, based on this information, is possible to make inferences about the dynamical nature of the system under study. These inferences can be made through calculation of the May-Sugihara Correlation Coefficient among predicted and observed time series through different prediction intervals, at an embedding dimension where the photometric time series is revealed as chaotic [8]. Finally, the Hurst exponent would allow the classification of the recorded dynamic systems according to their Brownian motion (i.e., ordinary or fractional Brownian motion) [10]. To evaluate the biological system with all the above quantifiers, photometrical time series of cells are recorded under shear stress in a steady state from RBCs samples of patients with CLL, ALL and IDA. The time series were obtained by Ektacytometry techniques using a device developed and patented by the Group of Applied Optics at Biology from IFIR (CONICET-UNR) [17,18]. For comparative purposes, the same procedure was carried out for healthy patients.

The second approach is based on the use of fractal dimension to digital analysis of images of RBCs after noise reduction with wavelet transform (WT). For simplicity, it will be referred to as **WT/BCD** method. In broad terms, a fractal could be defined as a geometric figure which exhibits similar patterns at different scales, i.e., a self-similar pattern. Frequently, the parameter used to measure the degree of self-similarity is the Fractal Dimension. Beyond the fact that several definitions of fractal dimension coexist [19], there is consensus that box counting procedure is an effective strategy to estimate it [20]. This technique can be applied to any data (i.e., points, curves, surfaces, etc.) to obtain the Box-Counting Dimension (BCD). Indeed, we have already applied this technique to distinguish different groups of RBCs according to their nature, discriminating healthy from ill RBCs incubated with *Ascaris lumbricoides* and *Trichinella spiralis* extracts [14]. WT is a time-frequency transform that decomposes an *n*-dimensional signal into a representation that shows signal details and trends as a function of time [21]. It is a unique tool for the treatment of problems related to real physical situations in which a signal contains discontinuities or sharp spikes [12,22,23]. In the present work, WT is employed for the

processing of images from RBCs in order to reduce noise prior to applying the box-counting method. It is expected that an appropriate wavelet transformation of the images would provide more reliable BCD values.

Both methodologies presented in this work allow us to elucidate the effects caused by IDA, CLL and ALL over the aggregation of RBCs. In addition, both approaches enable the differentiation between healthy and ill RBCs by using simple and non-invasive instruments.

2 MATERIALS AND METHODS

2.1 Red blood cells and digital image analysis

Every person involved in this work signed a medical informed consent form before participating. The ethics committee of the Universidad Nacional de Rosario has approved this project [24].

The samples of human venous blood of red blood cells of Group 0 were obtained from healthy donors, or with any of the pathologies studied (leukemia or anemia). A total of 40 samples were processed, 10 from healthy individuals, 10 from anemia patients, and 20 from leukemia patients (10 for CLL and 10 for ALL). They were preserved at 4ºC in a container with Na_2EDTA as anticoagulant until they were processed within 24 hours. Whole blood was centrifuged at 800 g during 10 minutes. Then, plasma and buffer coat were removed. The remaining RBCs were washed three times with phosphate buffer saline (PBS, pH 7.4, 295 ± 8 mOsmol / kg) at 25 ºC. Erythrocyte suspensions were obtained according to the protocols of the International Committee for Standardization on Hematology.

RBCs were suspended in 0.13% autologous plasma and maintained at rest for 5 minutes to allow aggregation. RBCs samples were examined in a concave optical inverted microscope slide (Union Optical, Japan). The photos for each of the samples (40 images in total) were obtained by duplicate with a digital camera (Canon Powershot A640, objective: 40X). The size of the images was 1280×960

pixels.

2.2 Time series

Time series were acquired with the Erythrocyte Rheometer (ER), an instrument based on the ektacytometry methodology. By means of the ER, quantitative information is obtained from diffraction particles, such as suspended RBCs, when subjected to light diffraction under Fraunhofer theory conditions [25].

The ER has two plane disks, both of them made by flint glass, superposed, coaxials, parallels, and horizontals. Suspensions of RBCs are placed between those disks. The driving motor is coupled to the lower disk by two helicoidally gears, allowing the rotational disk to start or stop rotation shortly. A dilute suspension of cells under shear stress takes a three-axial ellipsoidal shape, with the major axis in the same direction towards the shear field direction. Therefore, if a laser beam is passed perpendicularly through a thin layer of cells suspension, a Fraunhofer diffraction pattern is produced. The diffraction pattern is circular when the cells are at rest, and elliptical when they deformed by a shear stress field. The diffraction pattern is detected on a ground glass screen. A 5 mW HeNe laser as light source is used to perform this task. Diffracted intensity from long and short axes of the elliptical diffraction pattern falls inside a masked photomultiplier tube (PMT), after passing through a thin straight slot in the mask placed exactly on the corresponding axis of the elliptical pattern. The PMT signal output can be transmitted to a microammeter, where two values of electrical current can be measured. Finally, the data is stored for their processing in time series with 5461 points.

The time series can be divided into two portions, which relates to the moment when erythrocytes are subjected to shear stress [26-28]. For numerical methods, only the second part (3500 points) has been used.

Figure 1 shows a partial flowchart of the ER used to generate a typical time series for the creep process from healthy control samples obtained with the ER, as well as the Fraunhofer diffraction

patterns for rest condition and under shear stress. For further details, see the reference [17].
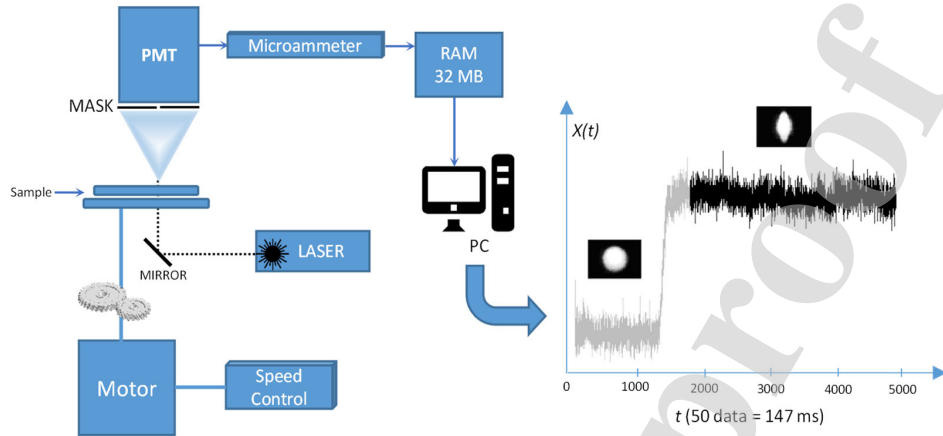
Figure 1. Partial flowchart of Erythrocyte Rheometer and a typical time series from the creep process of erythrocytes under shear stress and Fraunhofer diffraction patterns under shear stress. In the plot is shown the portion of the time series (the last 3500 points) that are used in our method (highlighted in black line).

2.3 Software

The algorithms for estimate the quantifiers were developed in two different programming languages, R [29] and MATLAB [30]; and are at disposal if required.

Images were processed with the software Fractalyse [31], in order to calculate the Fractal Dimension (BCD), according to an iterative principle based on the Box-Counting method. Before processing, the images were filtered using a Wavelet Toolbox [32] from MATLAB.

3   DATA ANALYSIS

3.1 MSH METHOD

The **MSH** method involves performing the following steps: (1) determining the embedding dimension (E) of the underlying attractor in the data series through the percentage of False Nearest Neighbors technique, (2) estimate the May-Sugihara coefficient from the E value, and (3) to use this

coefficient to calculate the Hurst exponent from each sample. The techniques used for the different steps of the method are well documented [7-9,33], therefore they are not discussed in detail here. Nonetheless, a detailed description of each technique is given in Supplementary Material section. Here is only presented a detailed description of the relation between the Hurst exponent and the May-Sugihara coefficient since this link is less explored.

Brownian motion is the random movement of the particles after colliding with the molecules in a fluid medium. Ordinary Brownian motion is among the most common stochastic processes and is closely related to the normal distribution. Its central feature is that the past increments in the particle displacements are uncorrelated with future increments. To describe this behavior is said that the system has no memory. On the other hand, in a correlated random walk (fractional Brownian motion), past displacements are correlated with future ones, at least for the first steps of the process. In some of these cases, there is a tendency to return to the place of origin hence the displacements become more intricate, leading to auto-intersections. Consequently, these systems have memory.

Hurst Exponent is a measure, which allows differentiating between time series from a random process and from one that has underlying tendencies, i.e., if time series portrays an ordinary or fractional Brownian motion [34]. This exponent is related to time-dependent functions $Y(t)$ according to:

$$Y(t) = \lambda^{-H}x(\lambda t) \tag{1}$$

where λ is a positive number and H is the Hurst exponent, which measures the type of correlation (positive or negative) when the increments are $\Delta Y(t_i)=x(t_{i+1})–x(t_i)$, whit x as the observed magnitude. The Eq. (1) indicates that the time series is self-affine since the fluctuations in different scales can be rescaled in order to obtain the original signal [35].

Jens Feder proposed a relation between the correlation coefficient of May and Sugihara ($<C_s(Y,Y^*)>$) and the Hurst exponent to processes that satisfy the self-affinity property [10],

$$< \mathbf{C}_s(\mathbf{Y}, \mathbf{Y}^*) > = \frac{<\Delta Y(t) \Delta Y^*(t)>}{<|\Delta Y(t)|^2>} = 2^{2H-1} - 1 \tag{2}$$

In Eq. (2), $<C_s(Y,Y^*)>$ is the correlation function between $\Delta Y(t)$ of the real series and $\Delta Y^*(t)$ for the predicted one, which is estimated as discussed in Supplementary Material section. As demonstrated by Mandelbrot [19] and as follows from Eq. (2), the value of the Hurst exponent is bounded between 0 and 1. In particular, if $<C_s(Y,Y^*)>$ is equal to 0, then $H = 0.5$. This result indicates that the increments in displacement are statistically independent, what is expected for ordinary Brownian motion. Otherwise, if $<C_s(Y,Y^*)> \neq 0$ indicates that one of the following situations may be occurring. On the one hand, past and future increments can be positively correlated. This behavior is described as persistent fractional Brownian motion. In that case, $H > 0.5$. On the contrary, if $H < 0.5$, past and future increments are negatively correlated. This behavior is known as anti-persistent fractional Brownian motion.

For further details on the techniques used to develop the MSH method, see Supplementary Material section. The algorithm for the estimation of the May-Sugihara coefficient (and R pseudo-code script) is also described in detail there.

3.2. WT/BCD METHOD

### 3.2.1 Box-Counting Dimension

If the analyzed images enclose a fractal pattern, i.e., basic fragmented or apparently irregular geometric structures are repeated at any scale. Then, it is possible to use that information to classify the samples. The fractal pattern can be measured through the Fractal dimension of the image. Although this cannot be exactly measured, several ways of doing so have been proposed [19,20,36,37]. In this work, fractal dimension is estimated through box-counting technique. For its implementation, the following generalization of the Euclidean dimension calculation is proposed:

$$N(L) \, L^D = 1 \Rightarrow D = \log(N(L))/\log(1/L) \tag{3}$$

where $N(L)$ represents the number of boxes of side L required to cover the object. For a geometric object of dimension 2, for example, a square, the equation is valid for $D = 2$ for any pair of L and $N(L)$. On the contrary, a fractal object does not satisfy the equation for an integer value of D. However, the box-counting dimension (BCD) can glimpse when the portions of the geometric shapes are accommodated and distributed in an image [36]. The potential fractal must be placed on a uniformly spaced grid, with cells of size L^2, and then it is counted how many boxes are required to cover the object. The BCD is obtained by refining the grid, according to Eq. (4):

$$D = \lim_{L \to 0} \frac{\log N(L)}{\log \left(\frac{1}{L}\right)} \tag{4}$$

Figure 2 illustrates the box-counting algorithm procedure. For their description are contrasted images from two samples of different nature: a healthy patient, and an IDA patient. Before processing, the images are binarized in black and white as required by the Fractalize software. The boxes required to cover the object are indicated as full boxes, while an empty box indicates that there is no information about the fractal object on it. The output is a plot where abscissas represent the values of the logarithms of reciprocal L, and ordinates correspond to the logarithm of N. Therefore, the slope of this log-log plot is the estimation of BCD.
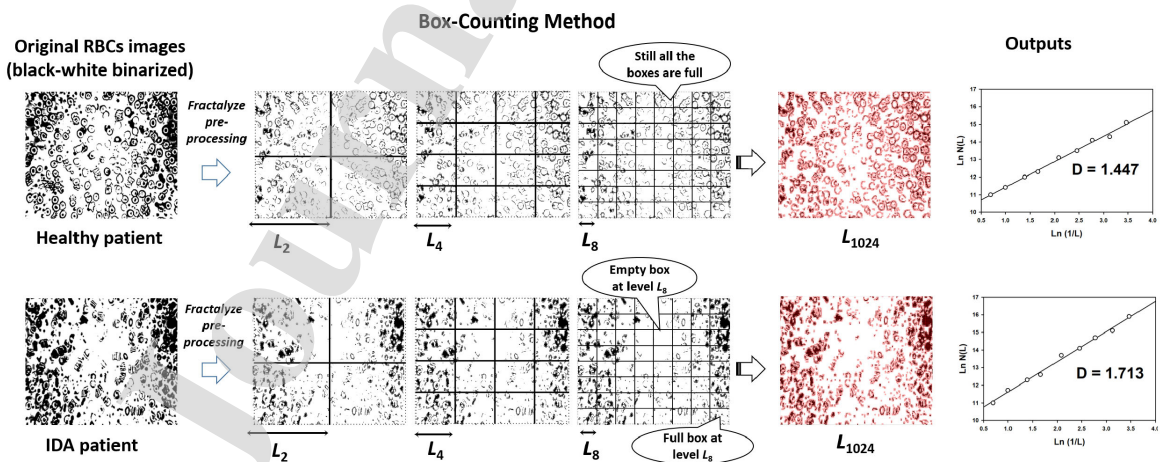
Figure 2. Schematic representation of the Box-Counting method applied to typical samples from healthy and IDA patients. For the binarized RBCs original images, Fractalize first modifies their contrast. Then, the method implements several guide-grid at different L levels in powers of 2 (from 2 to 1024) to build the corresponding Box-Counting plot. The highest value of L is bounded by the size of the processed image (1280×960 pixels).

3.2.2 Wavelet Transform

Wavelet transform is already a mature technique and is well documented [12], and therefore it is not described herein with much detail. It was chosen because in a preliminary analysis it was observed that certain artifacts or noise of the image could cause an error in the estimation of the BCD. The process to remove noise ("denoising") from an image is based on the decomposition of the data in a set of wavelets and then in the selection of a threshold value in order to select the appropriate coefficients to reconstruct the signal. Since wavelets find features in the data at different scales, it is possible to preserve important image details while removing noise. The central idea behind wavelet denoising –or wavelet thresholding– is that the wavelet transform leads to sparse representation for several real images, concentrating key image features in a few large magnitude wavelet coefficients. Small wavelet coefficients are noisy and are possible to remove without distorting the image. The data is reconstructed using the inverse wavelet transform after applying a suitable threshold to wavelet coefficients.

While there is no method to choose the wavelet that best fits each signal, the selection of the proper wavelet is an important factor to consider. In this work, bi-orthogonal wavelets (order 3, level 6.7) were used since they presented better results in the reconstruction of the images from their inverse wavelet transform without modifying the main features of the processed images.

4 RESULTS AND DISCUSSION

4.1 MSH method

The use of photometric series for the analysis of the deformability of RBCs is carried out by applying nonlinear quantifiers. They can determine if randomness is inherent to system dynamics or to measurement process, unraveling the noise from the relevant information and providing further insights into the underlying RBCs deformation mechanisms [13].

By the very beginning, the first differences $(x_{t+1} - x_t)$ were applied to clean the series in order to reduce the autocorrelation. Then, both the technique of time-delay coordinates proposed by Takens and the Abarbanel method of false nearest neighbors were applied to portrait the process dynamics in the proper phase space in the appropriate embedding dimension, as explained in Section 3 and Supplementary Material section. Figure 3 shows the %FNN of eight embedding dimensions consecutively increased for every sample. In all cases, when plotting the dynamics in a phase space of $E = 6$, the %FNN is below 1%. Therefore, the system attractor is completely unfolded for an embedding dimension of 6. From this value ($E = 6$), the May-Sugihara coefficient can be calculated. For further details about the link between the embedding dimension and the May-Sugihara coefficient, see Supplementary Material section.
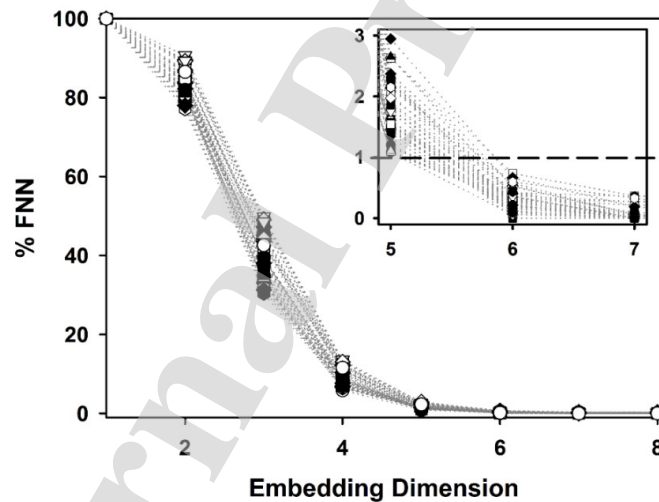
Figure 3. Embedding dimension E vs. %FNN. Inset: %FNN for $E = 5$, 6 and 7.

Figure 4 shows the May and Sugihara coefficients computed for the different samples at several correlation steps. It can be observed differences between RBCs samples from CLL when compared to IDA, ALL or healthy patients. When analyzing the second and third step, IDA and ALL samples provided lower correlation coefficients than CLL, showing a similar behavior to healthy samples (Fig. 4-B). By increasing the number of steps, that correlation can be distorted since the series could be dye

with uncorrelated additive noise.

(A)

(B)
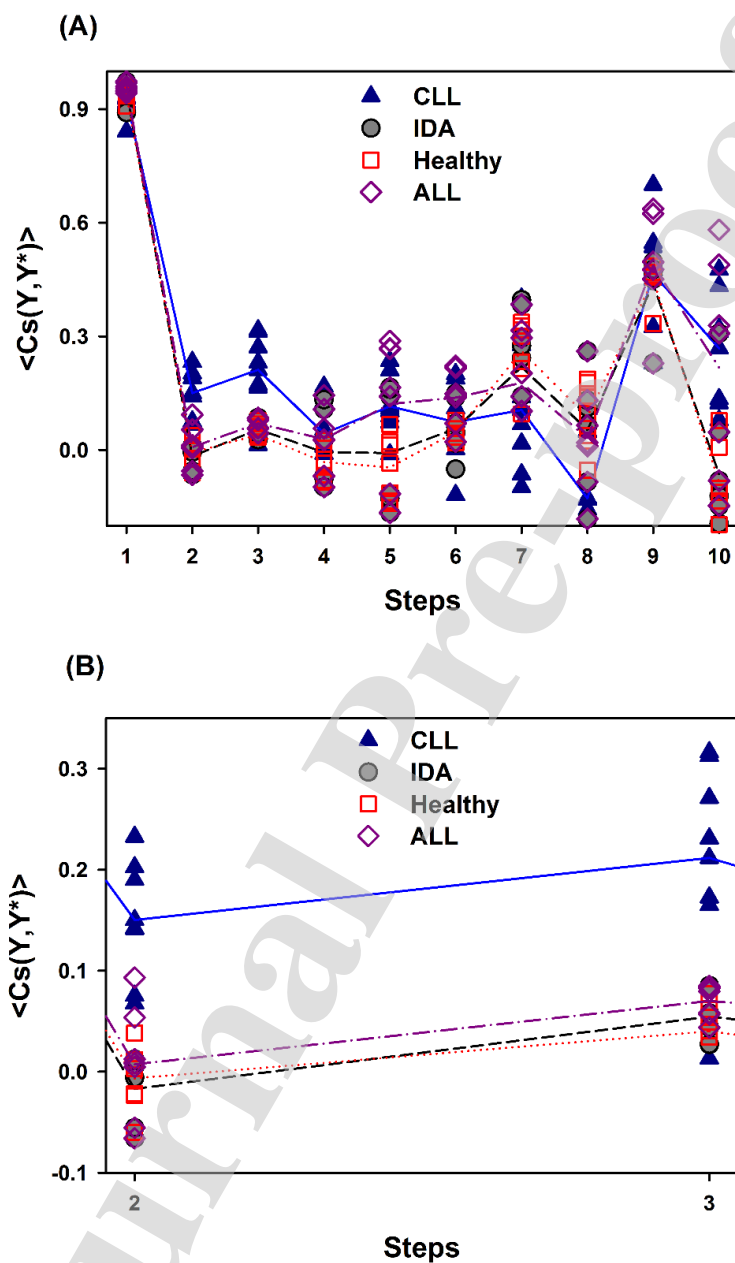
Figure 4. A) Correlation coefficient versus steps (*s*) for RBC from CLL (blue triangles), ALL (pink diamonds), IDA (gray circles), and healthy patients (red squares). Blue solid line, dash-dotted line, black dashed line, and red dotted line indicate the average values of CLL, ALL, IDA and healthy patients, respectively. B) The same figure, highlighting the step two and three. The embedding dimension used in each case was $E = 6$.

As a first interpretation, the fluctuations for the erythrocyte membranes subjected to a mechanical shear stress seem to have different behavior for the analyzed diseases. In fact, the prediction for IDA

or ALL samples, as measured by $<Cs(Y,Y^*)>$, indicates that there is no systematic dependence between experimental and expected values as s increases. By comparing this outcome with the behavior of healthy patients (Fig. 4, red squares, red dotted line), it is observed that the erythrocyte membranes affected by IDA or ALL have a very similar behavior to RBC membranes without injuries. On the other hand, for the CLL samples, the $<Cs(Y,Y^*)>$ does not decrease with increasing s. As seen above, this behavior is typical of a chaotic dynamic.

Table 1: Mean Hurst Exponent for all the RBC samples

Samples [a]	Hurst [b] (s=2)	Hurst [b] (s=3)	Hurst [b] (s=4)	Hurst [b] (s=5)	Hurst [b] (s=6)	Hurst [b] (s=7)	Hurst [b] (s=8)	Hurst [b] (s=9)
Healthy	**0.49**	0.54	0.47	0.46	0.53	0.67	0.56	0.77
	(0.02)	(0.01)	(0.03)	(0.06)	(0.02)	(0.05)	(0.06)	(0.03)
t [c]	0.58							
Leukemia								
(CLL)	**0.60**	0.63	0.53	0.58	0.55	0.39	0.77	0.67
	(0.04)	(0.07)	(0.06)	(0.05)	(0.08)	(0.12)	(0.08)	(0.09)
t [c]	6.68							
(ALL)	**0.50**	0.55	0.52	0.57	0.59	0.61	0.52	0.78
	(0.04)	(0.01)	(0.06)	(0.13)	(0.05)	(0.13)	(0.01)	(0.07)
t [c]	0.28							
Anemia								
(IDA)	**0.49**	0.54	0.49	0.49	0.54	0.63	0.53	0.76
	(0.02)	(0.02)	(0.07)	(0.11)	(0.05)	(0.14)	(0.10)	(0.05)
t [c]	1.22							

[a] The number of samples for each group is $n = 10$.
[b] Mean of Hurst exponents H. In parentheses, the standard deviation.
[c] Student's t to define if the average value of H for each sample group is significantly different of 0.5 for s=2. Critical t-value for n–1 degrees of freedom at a 95% significance level is $t_{crit(0.05,9)} = 2.26$.

Table 1 shows the mean Hurst exponents for all the RBCs samples from $s = 2$ to $s = 9$. Values of H for step 2 is highlighted. To corroborate whether the fluctuation dynamics of the RBC membranes have different Brownian behavior for each group of samples according to the H value for s=2, a Student t-

test was used. The null hypothesis corresponds to an ordinary Brownian motion (i.e., H ca. 0.5) while the alternative hypothesis corresponds to $H \neq 0.5$. The t values obtained for n-1 degree of freedom (where n is the number of evaluated levels) at 95% of significance for healthy, ALL, and IDA patients, agrees with the corresponding tabulated value ($t_{\text{crit}(0.05,9)}$ =2.26), that is, they are all less than this value. This means that for healthy, ALL and IDA patients the dynamics for the membrane fluctuations should be classified as an ordinary Brownian motion, where statistical properties such as invariance or range are not related at all. This result suggests that the injuries in the erythrocyte membranes produced by the IDA disease do not have a direct effect on the rheological properties of the blood, as shown in previous sections. On the contrary, for RBCs samples from CLL patients the observed t-value (6.68), indicates that the dynamic of the process could be described as a fractional Brownian motion ($H \neq 0.5$).

Also, a t-test was performed to determine the type of fractional Brownian motion corresponding to the LCC samples. In this case, the alternative hypothesis is $H > 0.5$ (i.e., fractional Brownian motion of a persistent nature). The statistical test result ($p < 0.01$) indicates that the LCC samples have a persistent fractional Brownian motion. The effect of this behavior causing a less dense diffusion than its ordinary Brownian counterpart. This result could indicate that the dynamics of the stress process provides useful information about how the evaluated disease can produce an alteration on the viscoelastic properties of the blood in a short time. In addition, a clear difference can be drawn in patients with leukocytic leukemia of different cell growth rates. Thus, it would appear that the injuries are not correlated with an alteration in the viscoelastic properties of the blood for patients with ALL. This result is in line with the previously discussed, i.e., the quick progress of the disease could prevent the processes that lead to morphological changes in the RBCs in those pathologies.

Finally, for values of s greater than or equal to 3, the relation between the dynamics of the process and the Hurst Exponent becomes less clear, as well as the coefficient of May and Sugihara. In all the studied samples, the erratic behavior of Hurst exponent for higher May and Sugihara Correlation values can be explained by the fact that the estimation of this one tends to lose correlation.

4.2 WT/BCD

In Fig. 5 are shown several images obtained from RBCs suspensions corresponding to blood samples from healthy patients, IDA and leukocytic leukemia patients. The first column presents raw pictures; the second column, the black and white transformed pictures, whereas the third column shows the pictures after applying a wavelet filter.
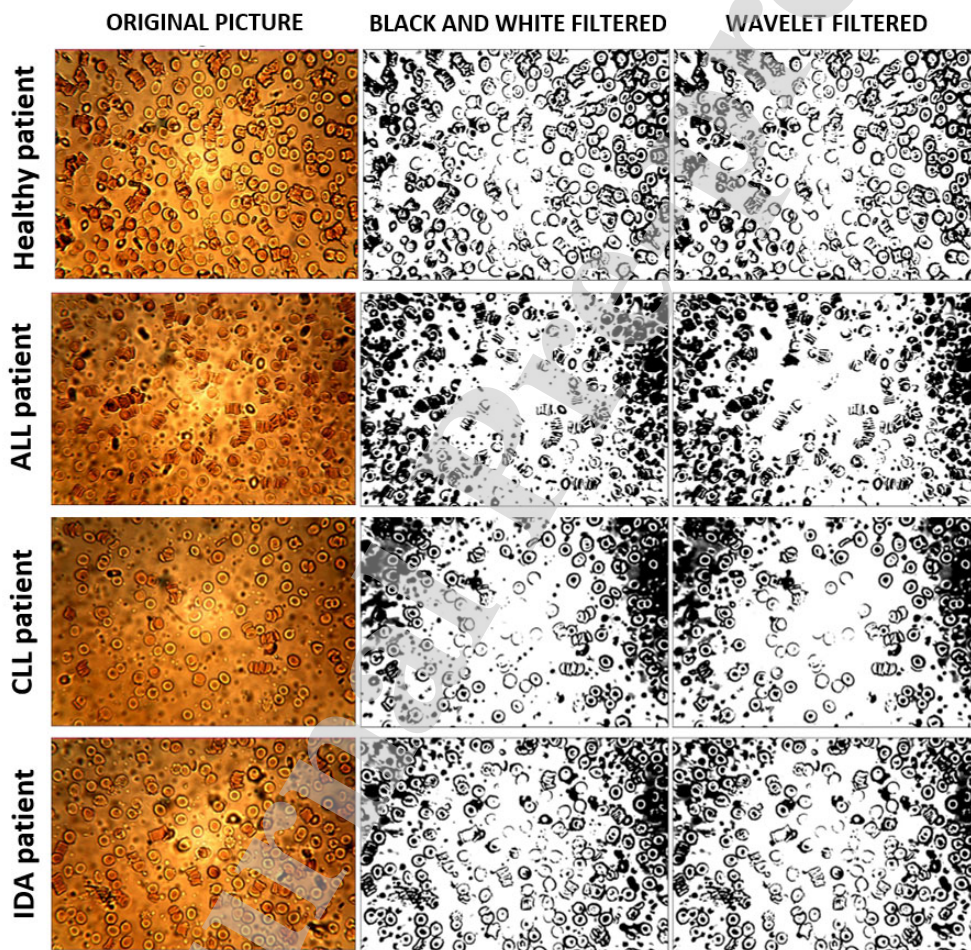

Figure 5. Images of several RBC samples, corresponding to a healthy patient, an ALL patient, a CLL patient, and an IDA patient at 40×magnification. The first column shows the original pictures, the second column shows the black and white processed images, as they are used in the box-counting algorithm, and the third column presents the same images filtered with the wavelet transform.

Black and white pictures do not show observable changes among the images corresponding to each group. However, as discussed below, the wavelet transform decreases the dispersion of estimated BCD

values since the noise reduction promote a decrease in the error of Box-Counting method, even though this result does not arise from the general image analysis. This outcome could allow a more appropriate classification of the samples according to the alteration caused by the studied diseases on the rheological properties of blood.

Figure 6 shows the box and whisker plots for BCD values obtained for RBC images from healthy and disease patients, processed with wavelet transform and without pre-processing step.
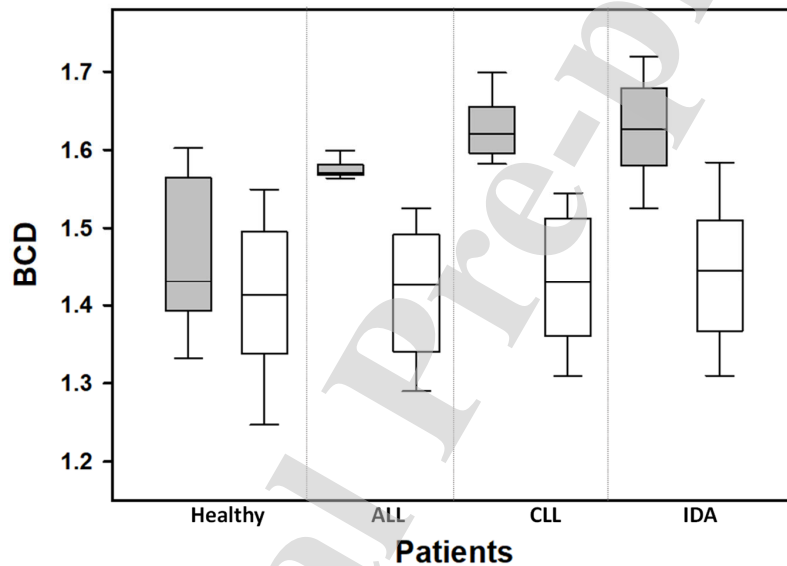
Figure 6. Box and whisker plots for Box-Counting Dimensions (BCD) obtained for RBC images from healthy and disease patients. Gray boxes correspond to the images processed with wavelet transform (WT/BCD), and the white boxes correspond to the same images without wavelet transform. For each case, the boxes are bounded by 25% and 75% quartiles with the median inside, whereas the extreme levels correspond to 5% and 95% quartiles.

In the first place, the results indicate that the processing of the images with the wavelet transform is an adequate option to differentiate the samples since the box and whisker plots corresponding to the BCD values of the transformed images indicate clear differences according to the examined patient group (gray boxes, Fig. 6). In contrast, the median BCD values of the untransformed images and their interquartile ranges are approximately the same for all sample groups (white boxes, Fig. 6).

According to the results of the **WT/BCD** method, there is an appreciable difference between the

medians BCD values of the healthy patients (1.42) and the disease patients (1.63 for IDA, 1.62 for LCC, and 1.57 for ALL). On the other hand, the interquartile ranges corresponding to the IDA, LCC, and ALL samples (0.10, 0.05, and 0.02, respectively) are lower than the samples of healthy patients (0.18). Besides, the first quartiles of these groups (1.58, 1.59, and 1.57, respectively) are higher than the third quartile of the healthy patients (1.56), which indicates that the **WT/BCD** method could discriminate the samples according to their nature or, at least, separate healthy patients from disease ones. At all events, it is verified that the wavelet transform can adequately fix artifacts in images that can lead to erroneous BCD measurements, as proposed above.

From these observations, three groups could be proposed: healthy RBC samples, ALL samples, and IDA-CLL samples. Statistical non-parametric tests were performed to test this hypothesis. Levene's test showed that the variances corresponding to IDA-CLL were statistically different ($p < 0.01$) from the ones obtained for the other samples, confirming our hypothesis. Dunn's test, however, allowed us to classify the samples in only two groups according to their BCD mean values ($p < 0.01$): IDA, CLL samples are grouped together and is proved that statistically differences appeared for healthy, and ALL samples.

In summary, the methodology described could be used to distinguish among different blood diseases that affect RBC through image analysis, even when these did not show noticeable visual changes. Interestingly, the Dunn's test suggests that the mechanical injuries that produce the chronic diseases on the RBCs are not observed in real diseases, as discussed in the introduction. The methods presented in this study suggest that acute leukemia does not produce significant changes in the behavior of the RBCs concerning the healthy patients used as control.

5 CONCLUSIONS

Two simple methods based on nonlinear analysis have been developed to explain the behavior of a complex biological system. Both proved to be helpful in the understanding of how several pathologies

affect the RBCs. Furthermore, their instrumental simplicity converts them into promising diagnosis alternatives.

Both methods complement each other to provide answers to the aims of the work. On one hand, it was possible to discriminate the type of blood disorder with a quantifier that measures the system degree of complexity by analyzing photometrical recorded series from erythrocytes subjected to shear stress. On the other hand, it was possible to discriminate samples according to their pathologies through analysis of fractal images.

Specifically, the **MSH** method links a dynamical process that describes the RBC membrane fluctuations, portrayed by a photometrical recorded time series, with an embedding dimension E, a correlation coefficient of May and Sugihara, and a Hurst Exponent. While all series have the same embedding dimension ($E = 6$), the other quantifiers yield promising results: the patients with CLL can be discriminated from healthy donors and patients with ALL and IDA. These results were obtained from the different patterns observed: chaotic behavior in CLL patients, in contrast to random dynamics for IDA, ALL and healthy control samples.

Finally, the **WT/BCD** method allowed us to statistically differentiate the IDA – CLL samples from healthy donors and ALL ones depending on their fractal aggregation patterns. Although it could be necessary to analyze more data to obtain reliable diagnostic information, this can be easily achieved since this method requires simple equipment (a non-professional camera), resulting in a viable alternative tool for screening and diagnosis in low-resources laboratories.

ACKNOWLEDGMENT

REFERENCES

[1] Chien S. Red cell deformability and its relevance to blood flow. Annu Rev Physiol1987; 49(1): 177–192.

[2] Korol AM, Foresto P, Darrigo M, Rosso OA. Diabetic erythrocytes test by correlation coefficient.Open MedInform J 2008; 2:105–11.

[3] Foresto P, D'Arrigo M, Carrera L, Etcheparre R, Valverde J, Rasia RJ. Evaluation of red blood cells aggregation in diabetes by computerized image analysis. Medicina 2000; 60:570–572.

[4] Miller KB, Daoust PR. Clinical manifestations of acute myeloid leukemia. In: Hoffman, R, Benz, EJ, Shattil, SJ, Furie, B., Cohen, HJ, Silberstein, LE, Mc Glave, P. eds. Hematology: Basic Principles and Practice. 4th ed. Philadelphia, Pa: Elsevier, 2005.

[5] Madu AJ, Ughasoro MD. Anaemia of Chronic Disease: An In-Depth Review, Med Princ Pract. 2017; 26:1–9.

[6] Nagababu E, Gulyani S, Earley CJ, Rifkind, JM, Mattson MP, Cutler, RJ. Iron-Deficiency Anemia Enhances Red Blood Cell Oxidative Stress, Fr2008; 42(9): 824–829.

[7] Takens F. Detecting strange attractors in turbulence. Dynamical systems and turbulence. Lec Not Math 1981; 1:366–381.

[8] Abarbanel HDI, Brown R, Sidorowich JJ, Tsimring LS. The Analysis of Observed Chaotic Data in Physical Systems. Rev Mod Phys 1993; 65:1331–1392.

[9] Sugihara G, May R. Nonlinear forecasting as a way of distinguishing chaos from measurement error in time series. Nature 1990; 344:734–741.

[10] Feder J. Fractals, Plenum Press, New York, 1988.

[11] Peitgen Hartmut HO, Saupe JD. Chaos and Fractals. New Frontiers of Science. Second Edition, Springer. 2004

[12] Mallat S, A wavelet tour of signal processing. Third Edition, Elsevier, USA, 2009.

[13] Mancilla Canales MA, Leguto A, Riquelme BD, Ponce-de-León P, Bortolato SA, Korol AM. Hurst exponent: a brownian approach to characterize the nonlinear behaviour of red blood cells deformability. Physica A 2017; 488:1–7.

[14] Lupo M, Leguto A, Bortolato SA, Korol AM. Evolution of erythrocytes aggregation: A fractal approach when incubated with Trichinella spiralis and Ascarislumbricoides. Ain Shams Eng J 2016 (doi: 10.1016/j.asej.2016.12.004).

[15] Rapa A. Fractal dimensions in red blood cell. Turk J Vet Ani Sci 2005; 29 (6):1247–53.

[16] Talu S, Stach S, Kaczmarska M, Fornal M, Grodzicki T, Burda W, Burda, K. Multifractal characterization of morphology of human red blood cells membrane skeleton. J Microsc 2016; 262(1):59–72.

[17] Riquelme B, Foresto F, D'Arrigo M, Valverde J, Rasia R. A dynamic and stationary rheological study of erythrocytes incubated in a glucose medium. Biochem Bioph Methods 2005; 62:131–141.

[18] Rasia, R.J., Quantitative evaluation of eruthrocyte viscoelastic properties from difractometric data: applications to hereditary spherocytosis and hemoglobinopathies, Clin Hemorheol Microcirc1995; 20:177–189.

[19] Mandelbrot BB. The Fractal Geometry of Nature. San Francisco: WH Freeman; 1983.

[20] Falconer K. Fractal geometry: mathematical foundations and applications. Third Edition, John Wiley & Sons; 2014.

[21] Sheng Y. The Transforms and Applications Handbook. CRC Press, 1996.

[22] Debnath L, Ahmad Shah F. Wavelet Transforms and Their Applications, Second Edition, New York, Springer, 2015.

[23] Wavelet transforms and their recent applications in biology and geoscience, Edited by Dumitru Baleanu, Intech, Rijeka, Croatia, 2012.

[24] Resolution number: 033/2015.

[25] Born M, Wolf E. Principles of Optics, 1999, 7th Edition, Cambridge University Press.

[26] Korol AM, Rasia R. Correlated random walk: a fractal approach to erythrocyte viscoelastic properties.ClinHemorheolMicrocirc1999; 20:97–103.

[27] Korol AM, Rasia R. Signatures of deterministic chaos in dyslipidemic erythrocytes under shear stress. Chaos 2003; 13:87–93.

[28] Korol AM, Foresto P, Rosso O. Self-organizing dynamics of human erythrocytes under shear stress. PhysicaA 2007; 386:770–775.

[29] R Core Team (2016). R: A language and environment for statistical computing. R Foundation for Statistical Computing, Vienna, Austria (http://www.R-project.org/).

[30] MATLAB. The Mathworks Inc., Natick, Massachusetts, USA, 2013.

[31] Vuidel G. Fractalyse software. Version 2.4. Available from: www.fractalyse. org.

[32] Wavelet Toolbox form MATLAB. The Mathworks Inc., Natick, Massachusetts, USA, 2013.

[33] Parker TS, Chua LO. Practical Numerical Algorithms for Chaotic Systems. Springer-Verlag, New York, 1990.

[34] Bagini F, Hu Y, Oksendal B, Zhang T. Stochastic calculus for fractional Brownian motion and applications, Springer, 2008.

[35] Simonsen I. Measuring anti-correlations in the nordic electricity spot market by wavelets. Physica A 2003; 322:597–606.

[36] Grassberger P. An optimized box-assisted algorithm for fractal dimensions. Phys Lett A 1990; 148(1–2):63–8.

[37] Fernández A, Schuster HG. Deterministic Chaos, VCH Verlagsgesellschaft, Weinheim. 273 Seiten, Preis: DM 108, Berichte der Bunsengesellschaftphysikalische. Chemie 1988; 92(9). 1059A-1060.

I have no conflict of interest